Available online at www.sciencedirect.com
ScienceDirect
Acta Materialia 57 (2009) 5718–5729
Acta MATERIALIA
www.elsevier.com/locate/actamat

The origin of non-uniform microstructure and its effects on the mechanical properties of a friction stir processed Al–Mg alloy

G.R. Cui, Z.Y. Ma *, S.X. Li

Shenyang National Laboratory for Materials Science, Institute of Metal Research, Chinese Academy of Sciences, Shenyang 110016, China

Received 6 May 2009; received in revised form 8 July 2009; accepted 31 July 2009
Available online 8 September 2009

Abstract

The microstructure of the stirred zone (SZ) resulting from friction stir processing or welding (FSP/FSW) has usually been assumed to be uniform when discussing the mechanical properties. However, numerous works have indicated that the fine-grained microstructures in the SZ were non-uniform, with precipitate, texture and grain size gradients caused by the severe plastic deformation and heat distribution. In this work commercial aluminum alloy 5083-H112 was subjected to FSP and fine-grained microstructures with an average grain sizes of 2.7–13.4 μm were obtained by controlling the FSP conditions. The stress–strain curves exhibited stepped yield point elongation, which was suggested to be associated with these characteristic non-uniform microstructures. Tensile tests indicated that the Hall–Petch relationship held in this FSP alloy when taking account of the average grain size. Toughness analysis indicated that the optimum toughness was anticipated to be obtained around a grain size of ~1 μm for this FSP alloy.

Keywords: Friction stir processing; Aluminum alloys; Grain refining; Mechanical properties; Yield phenomena

1. Introduction

Friction stir processing (FSP) has been developed as an effective grain refinement technique based on the principle of friction stir welding (FSW) [1]. It is well documented that the intense plastic deformation and temperature rise during FSW/FSP result in the generation of dynamic recrystallization, producing fine and equiaxed grains in the stirred zone (SZ) [2–4]. By changing the FSW/FSP conditions, such as process parameters, tool geometry, vertical pressure, composition of workpiece, temperature of workpiece and active cooling, a wide range of grain sizes from 0.1 to 17.8 μm can be produced by FSW/FSP [5].

When discussing the mechanical properties of FSP samples, as an approximation, the SZ is usually assumed to have a uniform microstructure [6]. However, numerous studies [7–12] have indicated that the SZ exhibits a non-uniform character, e.g. the grain size and texture vary with position. The grain size in the SZ tended to increase near the top of the SZ and to decrease with distance on either side of the center line [7,8]. Such a variation in grain size from the bottom to the top of the SZ is believed to be associated with differences in the temperature profile and heat dissipation.

In the microstructure produced by FSP onion rings, consisting of different scales of grains [9] and periodical microstructure with alternate particle-rich bands [7] have often been observed in cross-sections of the SZ or in horizontal cross-sections along the tool travel direction [10]. In a previous study [11] the flow lines induced by intense deformation also indicated a non-uniform microstructure like onion rings. Field et al. [12] indicated that severe gradients in crystallographic texture existed through the thickness and across the width of FSW joints and the character of local textures appeared to depend on the weld parameters. Also, Prangnell and Heason [10] found that the SZ material (thick 2195 Al alloy plate) had a strong ideal $\{1\,1\,2\}\langle 1\,1\,0\rangle$ texture or strong $B/\bar{B}$ ideal simple shear component, with the shear plane normal and shear

* Corresponding author. Tel./fax: +86 24 83978908.
E-mail address: zyma@imr.ac.cn (Z.Y. Ma).

1359-6454/$36.00 © 2009 Acta Materialia Inc. Published by Elsevier Ltd. All rights reserved.
doi:10.1016/j.actamat.2009.07.065

Table 1
Nominal chemical composition of Al alloy 5083 (wt.%).

Si	Fe	Cu	Mn	Mg	Cr	Zn	Ti	Al
0.4	0.4	0.1	~0.40–1.0	4.0–4.9	~0.05–0.25	0.25	0.15	Balance

direction being aligned approximately perpendicular to and tangential to the flow lines (surrounding the tool) in the SZ. However, there is still a lack of overall analyses on the origin, characteristics and influence of the non-uniform microstructure produced by FSP, especially for thick plates with a more apparent non-uniformity.

As experimental materials non-heat-treatable Al–Mg alloys have a simple element system and weakly anisotropic properties. Thus the mechanical properties of Al–Mg alloys are mainly determined by grain size and dislocation density. Lüders strain is one inherent feature of Al–Mg alloys with annealed fine grains, generally studied based on relative uniform materials [13], since it is well known that Lüders strain depends markedly on grain size [14]. The magnitude of Lüders strain increases as the grain size decreases. Considering the non-uniformity of FSP alloys, Lüders strain having different characteristics could be anticipated if the SZ consisted of grains which varied significantly. This could give some clues to a better understanding of the structure–property relations of FSP alloys.

In this work a non-heat-treatable Al–Mg alloy 5083 was used to investigate the effect of FSP conditions, such as FSP parameters, tool sizes, tool to workpiece angle and active cooling, on microstructure evolution and mechanical response. Especially, overall microstructure characterization in the SZ, based on grain size measurement and hardness tests, was carried out, and optimization of the material properties through grain refinement is discussed.

2. Experimental

Commercial aluminum alloy 5083 (H112) rolled plate 6.1 mm in thickness was used. The nominal composition of the as-received alloy is given in Table 1. The yield strength, ultimate tensile strength, uniform elongation and total elongation of the alloy are 205 and 337 MPa and 13.2% and 13.7%, respectively. The plates were cut into $6.1 \times 70 \times 400\ mm^3$ and were friction stir processed using a H13 steel tool. The tool was fitted with a threaded pin (right-handed screw). The FSP parameters used in this study and cooling systems are summarized in Table 2. The tool to workpiece angle was 2.5–3.5° from the vertical axis. For sample 9 a copper backplate and two narrow copper plates were placed under and on the workpiece, respectively, to increase the cooling rate. For sample 10, in addition to the copper backplate, fast flowing water covered the whole workpiece. Based on the FSP conditions, there are four main groups of samples for comparison, with differences in the (a) diameters of the shoulder and pin, (b) tilt angles, (c) rotation rates and travel speeds and (d) cooling methods.

Vickers hardness profiles were measured on a transverse cross-section (XOZ plane in Fig. 1) along the center line (OX), with a 200 g load for 15 s. The specimens for optical microscopy (OM), stereoscopy and electron backscattered diffraction (EBSD) were ground and electrolytically polished in a solution of 40 ml perchloric acid and 160 ml ethanol at −30 °C. The specimens for OM were anodized for 100 s at $0.4\ A\ cm^{-2}$ in Barker's solution – 5 ml HBF_4 (48%) in 200 ml water at room temperature. Tensile specimens with a gage length of 26 mm and a width of 4 mm were cut from the SZ along the FSP direction and thinned to 2.5 mm thickness, with the top and bottom parts being removed by an electrical discharge machine (Fig. 1). Tensile tests were conducted in an Instron 8871 tester at a strain rate of $1 \times 10^{-3}\ s^{-1}$.

3. Results

3.1. Microstructure

Fig. 2 shows typical optical microstructures of the SZ in the FSP samples, which were composed of fine equiaxed recrystallized grains. The grain size of the SZ could be adjusted by changing the size of the shoulder and pin, the rotation rate and travel speed of the tool and the angle of the tool to the workpiece or by using different cooling

Table 2
Tool size, FSP parameters and cooling methods used in this study.

Sample No.	Pin diameter (mm)	Shoulder diameter (mm)	Travel speed (mm min^{-1})	Rotation rate (r.p.m.)	Tilt angle (°)	Cooling method
1	8	20	150	300	2.5	Air/steel
2	8	22	100	400	2.5	Air/steel
3	6	18	200	400	3.5	Air/steel
4	6	18	200	400	3	Air/steel
5	6	18	200	400	2.5	Air/steel
6	6	18	300	500	2.5	Air/steel
7	6	18	400	600	2.5	Air/steel
8	6	18	500	700	2.5	Air/steel
9	6	18	200	400	3	Air/copper
10	6	18	200	400	3	Water/copper

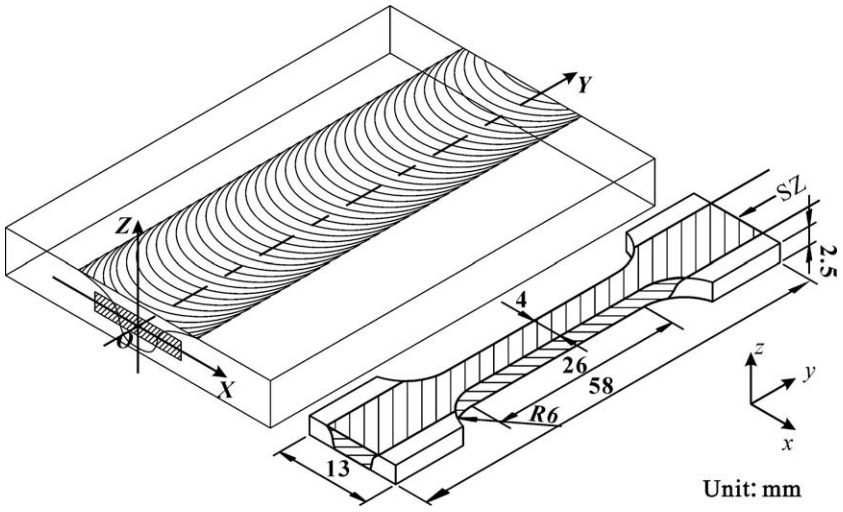

Fig. 1. Schematic illustration of the tensile specimen.

methods. As grain size is non-uniform across the SZ it was measured at five positions on the cross-section, as shown in Fig. 3a. The results are listed in Table 3. This shows that grain size in the SZ tends to be larger near the top (point 1) and smaller near the bottom (point 5). Grain size on the advancing and retreating sides did not show obvious differences and no consistent trend in variation was observed. It is important to note that the average grain size of the SZ was almost identical to that in the central zone of the SZ. It was found that the average grain size of the FSP samples generally decreased with decreasing the tool size, tool to workpiece angle and rotation rate/travel speed ratio, and with increasing the cooling rate.

3.2. Hardness profile

Hardness profiles along the center line (OX) of the SZ are shown in Fig. 4. They could be classified into four groups. Samples 1, 2 and 5 were prepared using different tools. As shown in Fig. 4a, the width of the low hardness zone of sample 1 was slightly smaller than that of sample 2. This is mainly due to a smaller shoulder on sample 1. A smaller shoulder and pin on sample 5 narrowed the low hardness zone further. However, the average hardness in the SZ of these three samples was almost identical. Samples 3–5, prepared with tilt angles of 3.5°, 3° and 2.5° exhibited average grain sizes of 8.1, 8.5 and 9.0 μm, respectively, in the SZ. As shown in Fig. 4b, sample 4 exhibited the most uniform hardness distribution, whereas sample 3 had the highest average hardness due to the finest grain size among these three samples.

Fig. 4c shows the effect of the rotation rate/travel speed (ω/v) ratio ($400/200 = 2$, $500/300 = 1.7$, $600/400 = 1.5$, $700/500 = 1.4$) on the hardness profiles. With increasing ω/v the width of the low hardness zone increased and the average hardness in the SZ decreased. Samples 4, 9 and 10 were prepared under different cooling conditions (cooling rate: air/steel < air/copper < water/copper). The faster the cooling rate, the smaller grain size. The SZ of sample 10 under water/copper cooling exhibited the highest hardness due to the finest grain size (Fig. 4d).

3.3. Mechanical properties

The relationship between the mechanical properties and average grain size of the FSP samples is shown in Fig. 5. It should be noted that the yield stress (YS) and ultimate tensile strength (UTS) increased with decreasing grain size, and they followed the Hall–Petch relationship (Fig. 5a):

$$\sigma_s = \sigma_0 + k_y d^{-1/2} \quad (1)$$

where σ_0 and k_y are constants. The elongation of the FSP samples tended to decrease slightly with decreasing grain size (Fig. 5b). It is impressive that sample 10 exhibited a higher tensile strength than the rolled base material (BM) almost without loss of elongation, even with the non-uniform microstructure induced by FSP.

Generally, the hardness (H_v) of a material is roughly proportional to the yield stress, and the relationship between H_v and grain size can be formulated as:

$$H_v = H_0 + k_H d^{-1/2} \quad (2)$$

where H_0 and k_H are constants associated with the hardness measurements. We noticed that hardness in the SZ had a somewhat non-uniform distribution, however, the relationship between average hardness and average grain size fits Eq. (2) well (Fig. 5c). Fig. 6 shows the variation in hardness against the grain size in the top, center and bottom zones of the SZ. k_H in the bottom zone was larger than that in the other two zones, which can be attributed to the faster cooling rate in the bottom zone.

3.4. Yield point elongation

Yield point elongation (YPE) (also called Lüders strain, a plateau in tensile curves) is a common phenomenon followed yielding in Al–Mg alloys, especially in fine-grained

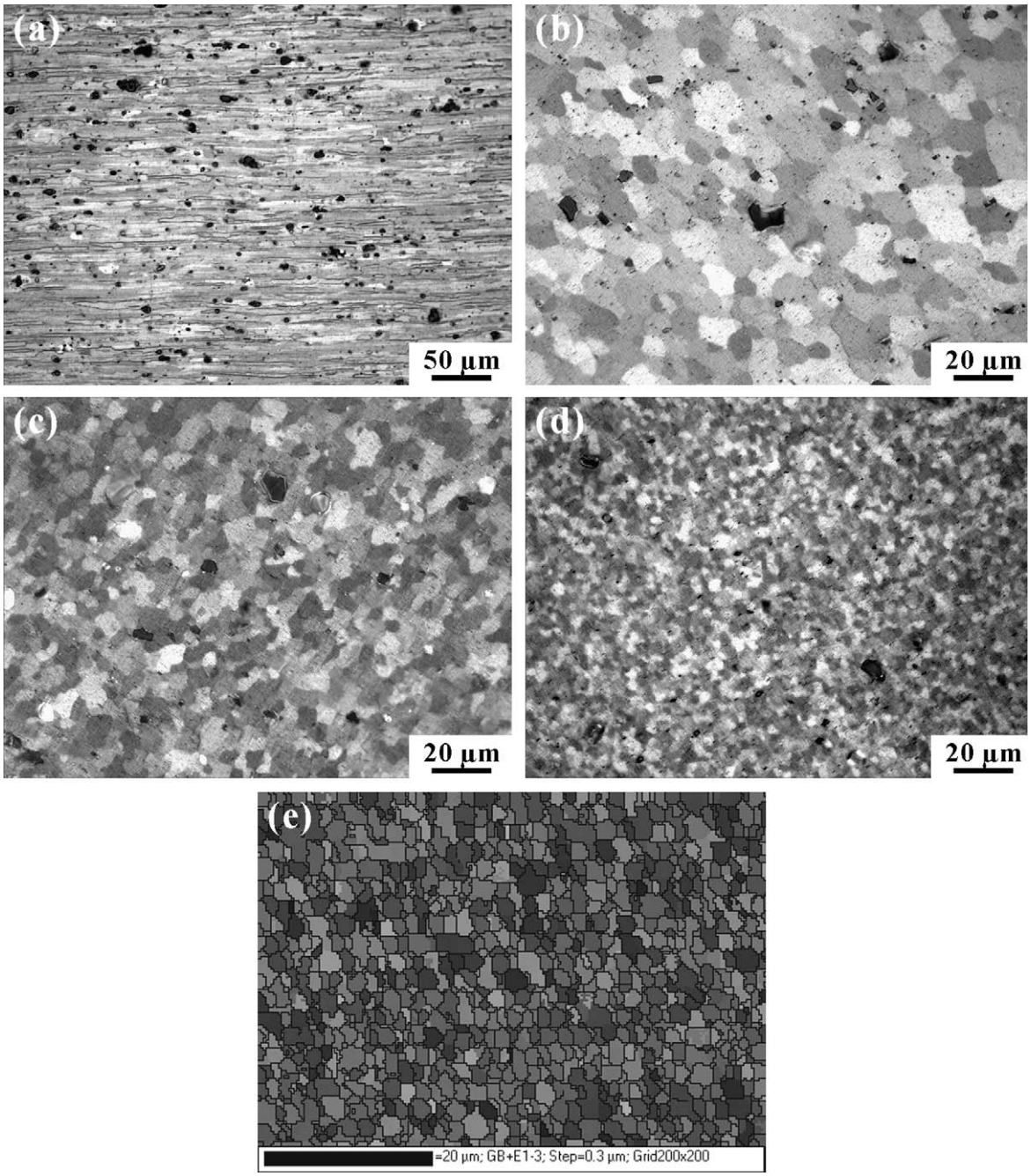

Fig. 2. Typical micrographs of fine grains: (a) base material; (b) sample 2, grain size $d = 13.4$ μm; (c) sample 5, $d = 9.0$ μm; (d) sample 9, $d = 5.0$ μm; (e) sample 10, $d = 2.7$ μm (measured by EBSD).

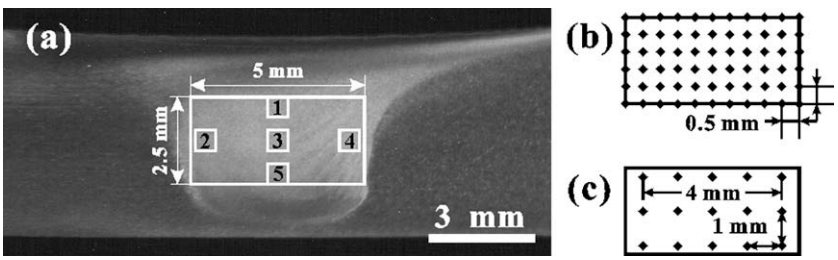

Fig. 3. Schematic positions in the central area of a transverse section (XOZ) for (a) grain size measurement, (b) dense hardness test in sample 10 and (c) sparse hardness test in all samples.

Table 3
Grain size (μm) at different locations in the stirred zones.

Sample No.	P1	P2	P3	P4	P5	Average
1	12.0	10.7	10.5	10.3	9.6	10.6
2	14.6	13.7	13.5	12.8	12.4	13.4
3	10.1	8.2	7.9	7.8	7.1	8.1
4	9.9	8.0	8.3	9.2	7.7	8.5
5	11.1	9.3	8.7	8.4	8.0	9.0
6	10.9	7.6	7.7	9.1	6.6	8.1
7	8.6	8.4	8.2	8.0	6.8	7.9
8	8.3	6.2	6.6	6.7	5.8	6.6
9	5.8	4.9	5.3	4.6	4.4	5.0
10			2.7(EBSD)			2.7

annealed alloys. It is usually attributed to the Mg solute pinning dislocations and dislocation multiplication [15], and is affected by factors such as grain size, strain rate, dislocation density, etc. In this study the tensile curves for all samples except the BM exhibited this phenomenon. However, some curves exhibited more than one step in this phase of YPE (termed stepped YPE). The typical tensile curve of sample 10 at a strain rate of $1 \times 10^{-3}\ s^{-1}$ is shown in Fig. 7, with arrows A, B and C indicating three steps, respectively. It should be noted that the stress increment between adjacent steps is ~10 MPa. Increasing the strain rate to $1 \times 10^{-2}\ s^{-1}$ increased the yield stress and the Lüders strain of the former two steps increased substantially, but the third step Lüders strain decreased, resulting in only a small increase in total strain. The yield stress of the first step at $1 \times 10^{-2}\ s^{-1}$ was close to the stress of the second step at $1 \times 10^{-3}\ s^{-1}$. The third step in YPE under two strain rates seemed to be a little slanted, and YPE and strain hardening in the third phase could not be as distinctly distinguished as in the first two phases. The effect of grain size on Lüders strain is shown in Fig. 8. As an approximation, Lüders strain is proportional to the reciprocal of grain size, as suggested by Lloyd and Morris [14].

3.5. Serrated yielding

Serrated yielding (also termed the Portevin–Le Chatelier (PLC) effect) in stress–strain curves is a common phenomenon in 5xxx aluminum alloys [16,17]. It is generally accepted that clouds of Mg solute atoms restrict dislocation motion and are responsible for the strain rate dependency of serrated yielding [18]. Serrated yielding was observed in all tensile curves in this study. During the tensile test serrated flow occurred after the yield point – the stress drop and serration intensity increased with strain. Furthermore, Fig. 9 shows that the stress drop increased and serration intensity (described by the average strain amplitude over the serration cycle) decreased with decreasing grain size. The data on stress drop and strain amplitude, to express the intensity of serrated flow, were average results for several cycles near the measuring point.

3.6. Comparison between stepped yield point elongation and hardness distribution

3.6.1. Transverse section (XOZ)

A dense Vickers hardness profile was built on the transverse section of the SZ for sample 10; the measured area was a little wider than the region from which the tensile

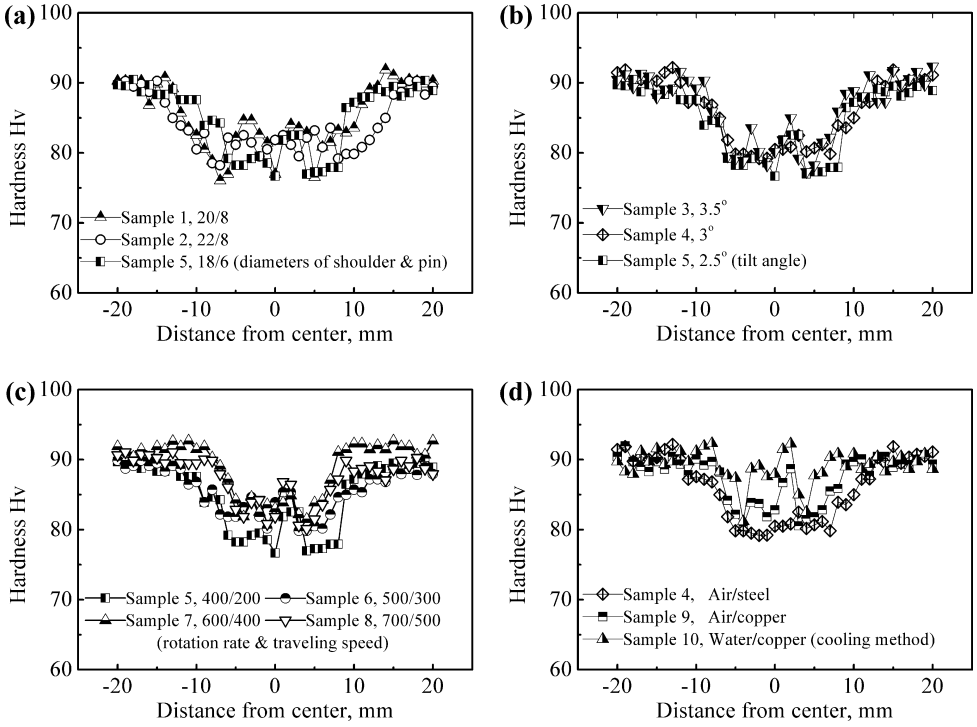

Fig. 4. Hardness profiles: (a) samples 1, 2 and 5 with different tools; (b) samples 3, 4 and 5 at different tilt angles; (c) samples 5–8 with different rotation rates and travel speeds; (d) samples 4, 9 and 10 with different cooling methods.

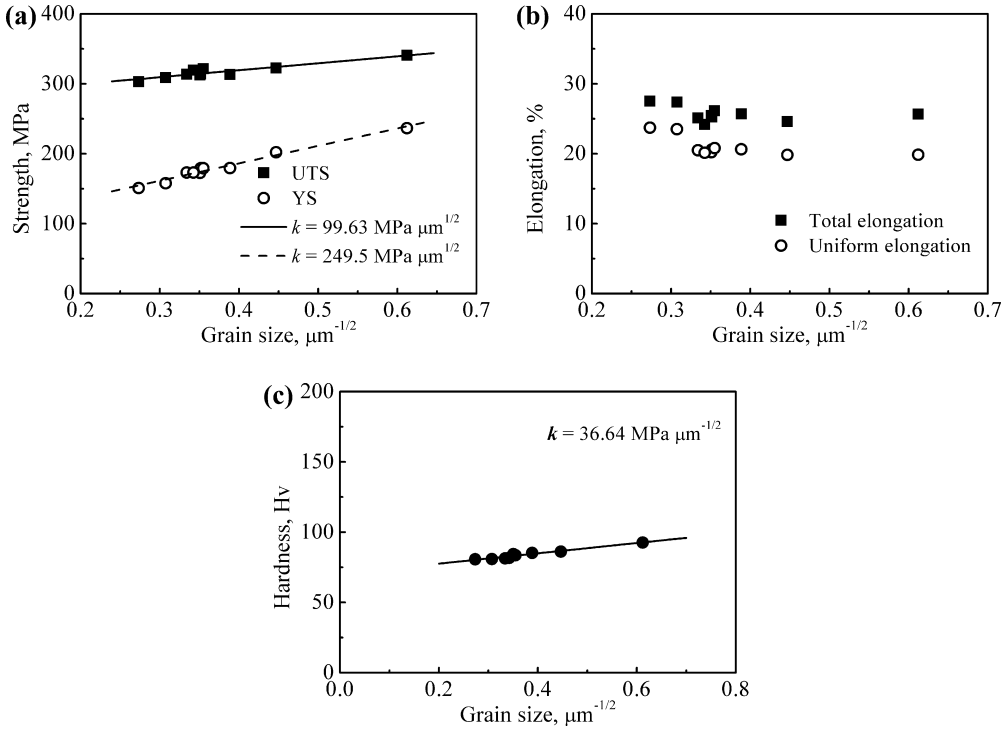

Fig. 5. Variation of (a) strength, (b) elongation and (c) Vickers hardness with $d^{-1/2}$ ($\mu m^{-1/2}$).

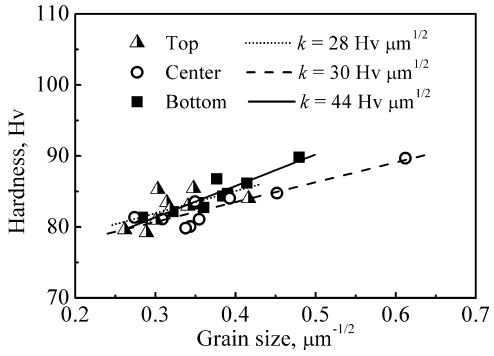

Fig. 6. Relationships between Vickers hardness and grain size at the top, center and bottom of the sampling area.

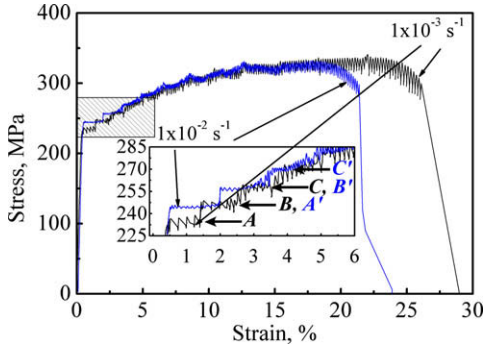

Fig. 7. Tensile curves of sample 10 under different strain rates. Note that three steps in yield point elongation are indicated by arrows for strain rates of $1 \times 10^{-3}\ s^{-1}$ (arrows A, B and C) and $1 \times 10^{-2}\ s^{-1}$ (arrows A′, B′ and C′).

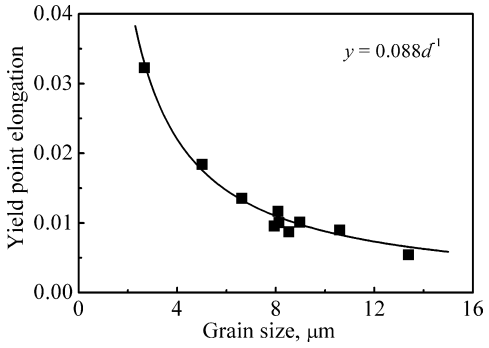

Fig. 8. Variation of yield point elongation with grain size.

specimens were machined (termed the sampling area). The exact points where hardness was measured are shown in Fig. 3b, and the resultant hardness profile is illustrated in Fig. 10. It should be noted that the hardness distribution was indeed non-uniform. The hardness values of the lower part of the SZ were significantly higher than those of the upper part.

In order to expedite the experiments all the FSP tensile samples were subjected to sparse hardness tests within the transverse section of the SZ at 15 points (see Fig. 3c). The tensile curves converged near the yield point and the corresponding hardness results are shown in Fig. 11, with the mean square deviation s for quantifying the non-uniform hardness distribution. According to Fig. 11, larger s values correspond to more steps in YPE. In this study, when $0.83 \leqslant s \leqslant 2.05$ one YPE was observed. With increasing s value, i.e. $2.1 \leqslant s \leqslant 3.86$, two or three stepped YPEs appeared.

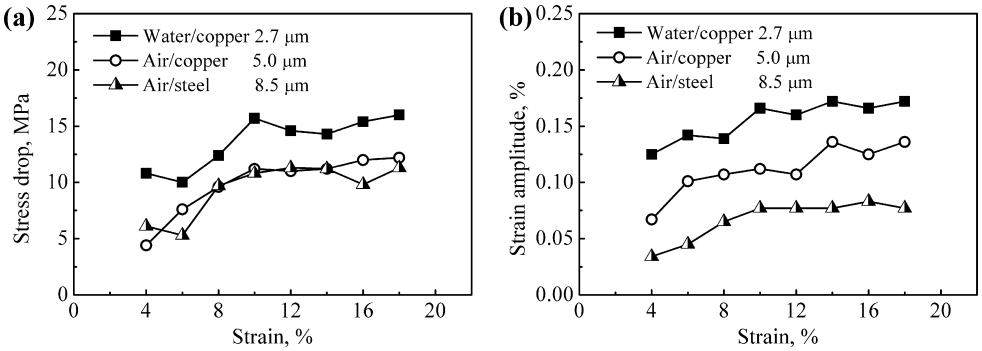

Fig. 9. Variation of serration flow with grain size and strain: (a) stress drop against grain size, (b) serration intensity (average strain amplitude of the serration cycle) against grain size.

3.6.2. Longitudinal section along the direction of travel (YOZ)

Fig. 12 shows the typical tensile curves of three FSP samples prepared under different cooling conditions. It was found that more steps in YPE were observed for samples prepared at faster cooling rates. Along the YOZ plane wavy patterns or onion rings could be found (Fig. 13). The onion rings were composed of wavy flow lines with periodic peaks at a spacing of ~500 μm that indicated traces of deformation. The generation of these flow lines has been discussed in our previous work [11]. The tensile specimens in this study were machined from the region between the two black lines (sampling area) in Fig. 13. For sample 4, with a slower cooling rate than the other two samples, the etched flow lines were distinctly visible (Fig. 13a) and, correspondingly, the onion rings, which consisted of arranged flow lines, were distinct. For sample 9, with a faster cooling rate, most of the flow lines were blurred with only a few being sharp and, therefore, the onion rings also looked blurred (Fig. 13b). Sample 10, with the fastest cooling rate, showed few sharp flow lines and most could not be discerned and, therefore, the onion rings could only be distinguished from a few sharper flow lines (Fig. 13c). These onion rings and wavy flow lines were in fact three-dimensional structures and they distributed in the whole samples. The flow line zones with higher hardness values could be considered as spatial wavy layers in the samples.

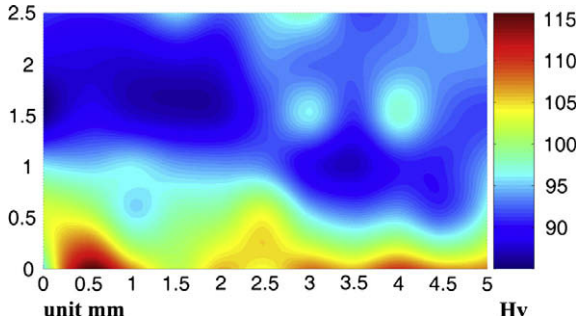

Fig. 10. Vickers hardness distribution in the cross-section corresponding to Fig. 3b.

As stated above, the upper half part of the sampling area was softer than the lower half part, therefore, more attention was paid to the lower half, which corresponds to the locations of the sharp flow lines in Fig. 13b and c. As the onion rings and wavy patterns are periodic structures, the hardness distribution in one period could provide a general understanding on the structure. For the periodical microstructure distribution (500 μm per period) any local property distribution at the same location in each period is identical. To avoid interference by indentations at two adjacent points at an interval of 50 μm in a period, an actual hardness test interval of 450 μm was adopted. The Vickers hardness results and modified test points in sample 10 which showed three steps in YPE are shown in Fig. 14. The arrows indicate that the test points with relatively higher hardnesses are located in the flow line zone, i.e. the wavy layer. This means that the wavy layer shows greater hardness than the adjacent region, and it may be considered that a hard wavy layer was embedded in a soft matrix. From the hardness distribution stated above it could be concluded that the hard wavy layers are mostly located in the lower part of the sampling area.

4. Discussion

4.1. Effects of FSP parameters on microstructure and hardness distribution

Generally, the average grain size of the FSP 5083 samples decreased with smaller tools, a lower rotation rate, a higher travel speed and more efficient cooling (Table 3). These conditions exerted their effects by decreasing the heat input and increasing the cooling rate during FSP. Smaller tools and a lower ω/v ratio reduced friction heat due to a decrease in the contact area between the tool and workpiece and the tangential velocity. A greater tool to workpiece angle tended to increase the forging force at the shoulder, thereby increasing the strain and friction heat. The combined effects decreased average grain size. Intensified cooling not only accelerated heat dissipation, but also reduced the rise in temperature, thereby inhibiting growth of the grains.

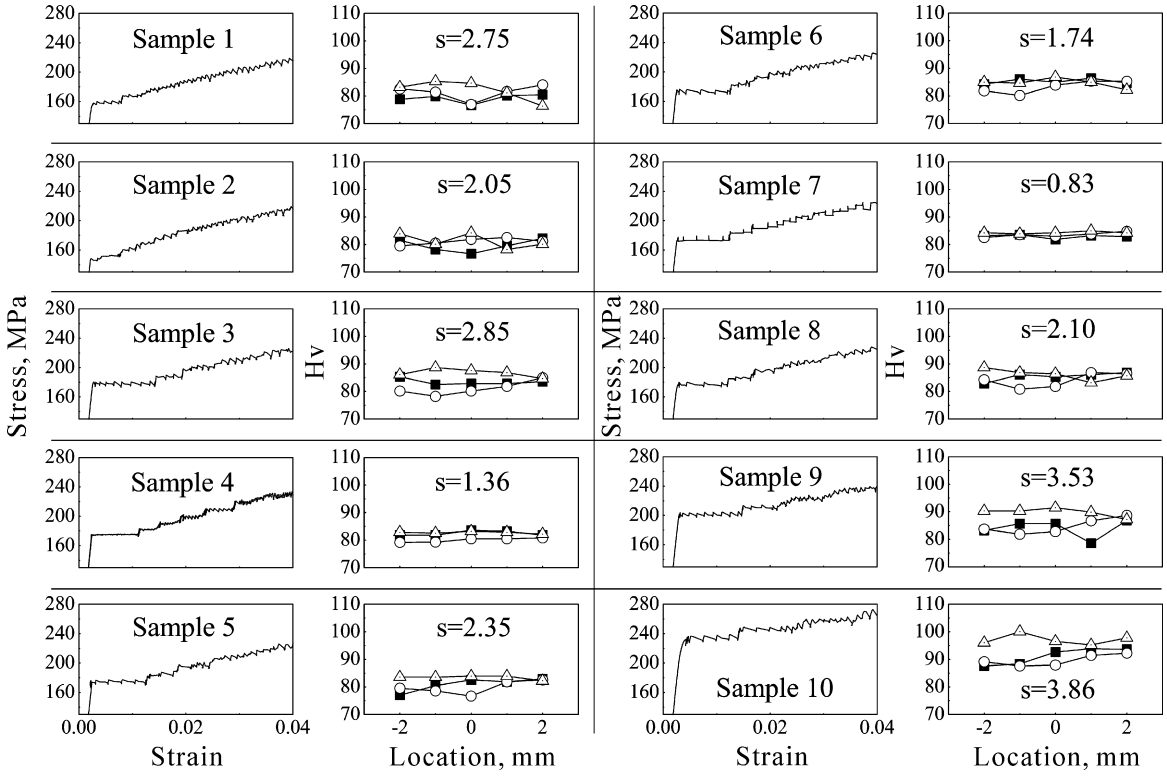

Fig. 11. Tensile curves near the yield point (left) and hardness distribution in the central area of the cross-section and the mean square deviation (s) of hardness (right). Solid square, open circle and open triangle indicate hardness at the top, center and bottom of the SZ, respectively.

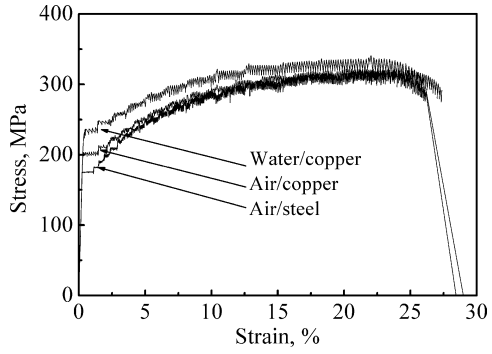

Fig. 12. Typical tensile curves of FSP 5083 samples for different cooling methods (testing strain rate: $1 \times 10^{-3}Sv^{-1}$).

The grain size and hardness distributions in the SZ had an apparent gradient from the top to the bottom. Such a variation is believed to be associated with the temperature distribution. Heat generation and dissipation during FSP showed obvious differences between different regions in thick workpieces. The tool shoulder produced most of the heat and a greater strain at the top than that at the bottom. The bottom of the workpiece was in contact with a backplate which acted as a heat sink that lowered the peak temperature and reduced the time at at high temperature. Thus, grain growth in the bottom of the SZ was effectively retarded during FSP. Especially in this study, the higher cooling rate due to the copper backplate intensified the effects of retarding grain growth, which made the grain size difference between the top and bottom more obvious than when using steel plates. Further, water cooling enhanced such a retarding effect. While the grain size in the SZ could be changed by using different FSP conditions, the grain size in the central location could be simply denoted as the average grain size (Table 3).

Mahoney et al. [19] conducted a detailed examination on grain size in various regions of the SZ of 6.35 mm thick FSP 7050Al. They revealed that the average grain size ranged from 3.2 μm at the bottom to 5.3 μm at the top and 3.5 μm from the retreating side to 5.1 μm on the advancing side. The grain size distribution from the top to the bottom of the SZ for the FSP 5083 samples was similar to that for FSP 7050 Al [19]. However, the grain size distribution from the retreating side to the advancing side in this study is different from that in Mahoney et al. [19]. As discussed above, it is well documented that the bottom of the SZ experienced a lower temperature and shorter excursion time than the top, thereby producing a smaller grain size. However, there is still controversy about the temperature profiles of the retreating and advancing sides, i.e. which side had a higher peak temperature during FSW/FSP. While it was reported that the advancing and retreating sides experienced different peak temperature during FSP/FSW [20], Tang et al. [21] showed that thermocouples placed on the advancing and retreating sides at equal distances from the weld seam of 6061 Al-T6 showed no significant differences in temperature. Similar grain sizes on the advancing and retreating sides for FSP 5083 Al implied that the temperature profiles

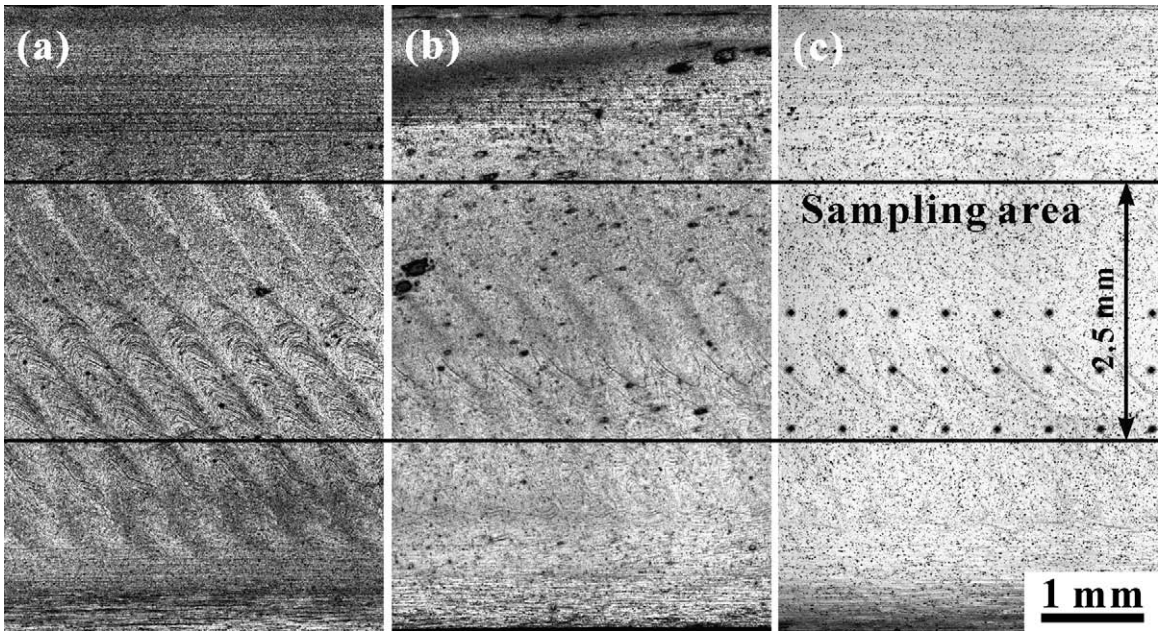

Fig. 13. Macroscopic view in longitudinal section of FSP samples for different active cooling conditions: (a) air/steel; (b) air/copper; (c) water/copper.

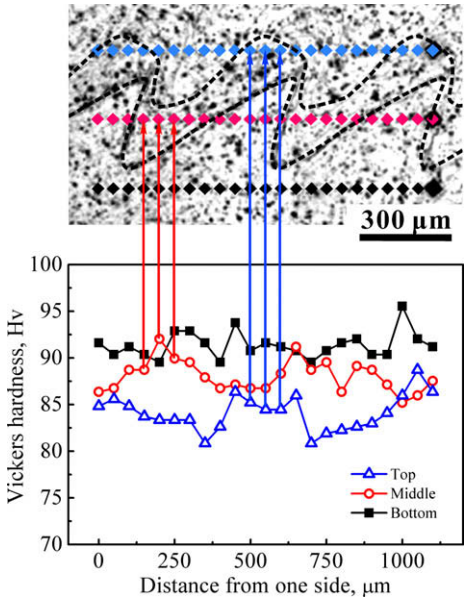

Fig. 14. Vickers hardness results for the flow line zone (wavy layer) in a longitudinal section of sample 10. The arrows indicate where the test points located in the wavy layer (demarcated by the two black dash lines) have relatively greater hardness.

on the two sides might be quite similar during FSP. This requires further experimental examination.

The severe plastic deformation and heat input produced fine equiaxed grains by dynamic recrystallization (DRX) [22]. Three types of DRX mechanisms have been proposed for FSW/FSP, i.e. discontinuous DRX (DDRX), continuous DRX (CDRX) and geometric DRX (GDRX). These mechanisms can occur synchronously and their respective contributions are difficult to isolate on the basis of experimental data [23]. In this study the grain size ranged from 2.7 to 13.9 μm, but the grain morphology showed no apparent differences. Specifically, the results for samples 4, 9 and 10, which were prepared under almost the same conditions except for process temperature, indicated that the grain size difference was caused by cooling effects.

Active cooling as an effective method to reduce the extensive growth of recrystallized grains has been used to obtain very fine grains by Su et al. [3]. In their work a small pin with a length of 1.9 mm was used. For the thicker plates the cooling could not exert the same effect on the whole thickness, but could still retain some dislocations in part of the SZ. Similarly, Jata and Semiatin [24] reported that DRX during FSW often left some grains with a high density of dislocations in the SZ. In this work most of the SZ contained inhomogeneous grains, while the area with the higher cooling rate had a higher dislocation density than the area with the lower cooling rate. Ito et al. [25] suggested that the larger k_H value was attributable to a high density of dislocations in the ultrafine grains produced by the especially intense straining processes. Sato et al. [26] investigated the hardness of FSW 5083 samples produced without active cooling and found that the Hall–Petch slope for hardness variation with grain size was 34 $H_v\ \mu m^{-1/2}$, almost same as the average results (37 $H_v\ \mu m^{-1/2}$) in this study, as shown in Fig. 5c. The results in the top (28 $H_v\ \mu m^{-1/2}$) and middle (30 $H_v\ \mu m^{-1/2}$) zones were lower than that (44 $H_v\ \mu m^{-1/2}$) in the bottom region, which underwent faster cooling, as shown in Fig. 6. Thus, this phenomenon indicated that the dislocation density in the bottom part was higher than that in the other two parts. This observation also indicated that the dislocation density distribution is a structural heterogeneity, as is the grain size gradient.

4.2. Relationship between stepped YPE and hardness distribution

For the FSP samples the SZ was characterized by fine recrystallized grains. Thus, it is not surprising that YPE was observed in the stress–strain curves. However, this stepped characteristic is different from conventional results. Generally, uniform materials have been used to study YPE, except for an Al–Mg alloy with duplex grain sizes, which was reported to exhibit a stepped characteristic during the whole plastic deformation phase in the tensile curves [27]. However, this stepped characteristic only occurred in the YPE phase, i.e. during Lüders band propagation in this work. This stepped characteristic raised the question of how the single Lüders strain was divided into two or more phases. Generally, the process of Lüders band propagation is understood as dislocation generation within the band and the introduction of dislocations into adjacent regions a short distance ahead of the band front. Thus, the beginning and end of Lüders strain depended on the resistance of the introduction of dislocations, due to unyielding grains. It is possible that some structural differences (grain size and dislocation non-uniformity) caused discontinuity in the Lüders strain.

Fujita and Miyazaki [28] indicated that Lüders strain began in trigger grains affected by long range interactions between individual grains, and when the applied stress reached a certain value the trigger grains would deform irrespective of their orientation factors. After the start of Lüders strain, stress concentration at the front ledge of trigger grains (termed the affected zone) impelled the adjacent grains to yield at the same applied stress value, and macroscopic views could be observed at this time. However, constrained by the stress concentration factor of the front ledge and starting yield stress, some areas with higher yield resistances, caused by a smaller grain size or higher dislocation density, could be bypassed in the propagation of Lüders strain unless the strain compatibility required by the deformation increased the stress concentration on the unyielding grains. The hardness value could be considered as the yielding resistance of the grains. It was found that the number of steps increased with an increase in the standard deviation of hardness statistic (Fig. 11), which is a measure of the grain yielding resistance variation. Therefore, it is suggested that hardness non-uniformity is a prerequisite to stepped Lüders deformation.

In considering the effects of the hard wavy layers on Lüders strain one should inspect the interaction between Lüders strain propagation and one wavy layer for simplicity, as schematically illustrated in Fig. 15. The coarse gray curve indicates the profile of the wavy layer in the sample. Lüders strain began in the upper half part of the sampling area and propagated in the cross-section first, to satisfy deformation compatibility. However, the wavy layer blocked propagation due to its greater hardness. And there were associated soft zones adjacent to the wavy layer, as indicated by the circles in Fig. 15. The circled zone above

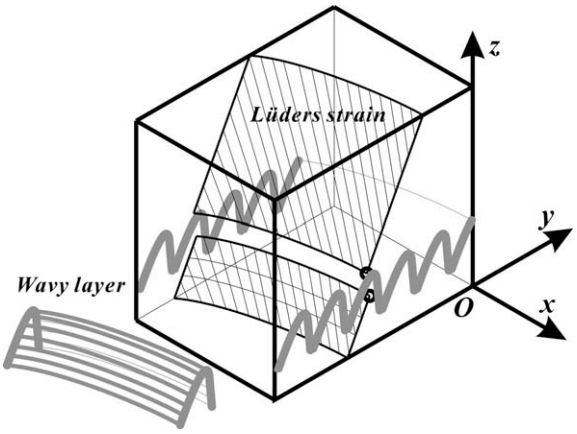

Fig. 15. Schematic illustration of the interaction between Lüders strain propagation and the wavy layer in the cross-section of a sample.

the wavy layer would yield when Lüders strain was applied, while the circle zone below the wavy layer would propagate a new wave of Lüders strain, due to its lower hardness. Thus, two separate bands of Lüders strain propagated together in the cross-section, maintaining deformation compatibility during subsequent propagation in the tensile direction. The wavy layer could deform like a spring, keeping up with other zones showing elastic deformation. When the first phase of Lüders strain ended, after a little strain hardening, the wavy layer might start a second phase of Lüders strain. Transient strain hardening between these phases increased the stress, and then the stepped characteristic appeared in the curves. If the wavy layer had a great enough hardness gradient, there was probably a third phase of Lüders strain. The special wavy layer supplied a structural factor for stepped Lüders strain.

Many pioneering results [28–30] have shown that for a given grain size increasing the strain rate will increase the Lüders strain. In this study increasing the strain rate induced an increase in the first two phases of Lüders strain, while the third phase decreased. Increasing the strain rate generated more dislocations, and the yield stress increased. Thus, the stress concentration at the front ledge of the trigger grains would increase and the range of grain size involved in Lüders strain propagation would increase too. Thus, the first two phases of Lüders strain would include more grains and the corresponding strain would also increase, while the last phase of Lüders strain would be shorter because there were few remaining grains. If the strain rate increased above a certain value the yield stress and stress concentration factor might increase to a level high enough to cover the hardest zone, and then there would be only a single plateau in the tensile curve, i.e. the stepped phenomenon would disappear.

As the second phase of Lüders strain proceeded the yielding zone would be hardened by the force of deformation compatibility. This would gradually increase the stress of the Lüders strain and induce a mixture of subsequent Lüders strain and strain hardening. The plateau would be slanted and it would be difficult to distinguish Lüders strain

and uniform strain hardening. Thus, the last phase of Lüders strain in sample 10 was difficult to discern in the tensile curve.

4.3. Effects of grain size on serrated yielding

Serrated yielding was observed in all tensile curves of the FSP 5083 samples. Only a small fraction of grains in the SZ had a high density of dislocations; most were similar to those produced by ultimate annealing. In tensile tests plastic deformation produced a large number of forest dislocation, which hindered mobile dislocations, thus serration intensity decreased and the stress drop increased as deformation proceeded. Wen and Morris [31] observed a similar phenomenon in AA5182 alloy produced by cold rolling and annealing. However, a greater stress drop and higher serration intensity in the stress–strain curve were observed for samples having a smaller grain size than those having larger ones [31]. As shown in Fig. 9b, the present results indicate an opposite possibility for serration intensity.

4.4. Optimum tensile properties

The tensile properties of a material are measured as yield strength (σ_s) or UTS (σ_b) and uniform elongation (ε_u) or total elongation (ε_t). In most engineering applications both high strength and high ductility are desired. Unfortunately, it seems that materials may be strong or ductile, but rarely both at once. Since both high strength and high ductility are essential, toughness (a combination of appropriate yield strength and uniform elongation) (T), partially represented by the work applied per unit volume before necking in the tensile test, is defined as [32]:

$$T = \sigma_s \varepsilon_u \tag{3}$$

The grain size dependence of the uniform elongation ε_u can is given by [32]:

$$\varepsilon_u = \varepsilon_0 - \frac{1}{A + Bd} \tag{4}$$

where ε_0, A and B are the experimentally determined material parameters and d is the grain size in μm. Hayes et al. [33] investigated the effect of grain size on the tensile behavior of a submicron grained Al–3 Mg alloy produced by equal channel angular extrusion (ECAE) and subsequent annealing. In this study we considered that the variation in uniform elongation with grain size might be similar for Al–3 Mg and Al–4.5 Mg (5083), i.e., the uniform elongation of 5083Al could also approach zero when the grain size was below a certain small value, like Al–3 Mg. The dependence of the uniform elongation of 5083Al on grain size could be fitted to Eq. (4) (Fig. 16a).

By combining Eqs. (1), (3), and (4), the toughness can be given as:

$$\begin{aligned} T &= \sigma_s \varepsilon_u \\ &= (86.48 + 249.5/d^{1/2})[24 - 1/(0.013 \\ &\quad + 0.08d)]/1000 \end{aligned} \tag{5}$$

The toughness increased with decreasing the grain size, then decreased when the grain size was below a certain value, as shown in Fig. 16b. Sample 10, with a grain size of 2.7 μm, had the maximum toughness of all tested samples. It should be noted that a toughness peak would appear if smaller grain sizes were obtained in the shadow grid zone (Fig. 16b). The optimum toughness was anticipated to be obtained at a grain size of ~1 μm for FSP 5083 Al.

5. Conclusions

The grain sizes and hardnesses in the SZ produced by FSP were not uniform. Adjusting the processing parameters, tool dimensions and cooling method changed the average grain size in the SZ, while changing the grain size and hardness distributions within the whole SZ.

Although the microstructures in the SZ were non-uniform, the average grain size was almost equal to that of the central zone, and the Hall–Petch relationship still held and total yield point elongation was inversely proportional to grain size.

Yield point elongation in the FSP samples showed a stepped characteristic in the tensile stress–strain curves. Hardness non-uniformity was a prerequisite, and a hard wavy layer was the structural factor.

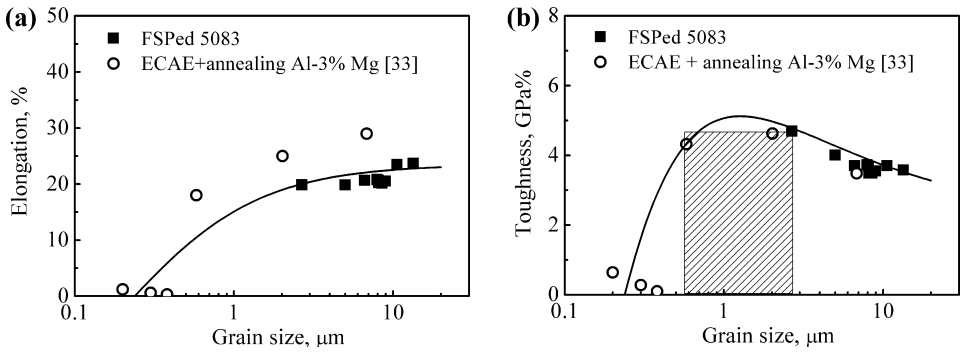

Fig. 16. Effect of grain size on (a) uniform elongation and (b) toughness (GPa%).

After serrated flow occurred after the yield point, the stress drop and the serration intensity increased with strain. The stress drop increased and serrated intensity decreased with decreasing grain size.

A FSP 5083 Al alloy with a grain size of 2.7 μm exhibited higher strength and elongation than the as-rolled base material. Toughness analysis indicated that there is the potential to produce a fine-grained 5083 alloy by FSP with optimum toughness.

Acknowledgments

The authors gratefully acknowledge the support of the National Natural Science Foundation of China under Grant Nos. 50890171 and 50471082, the National Basic Research Program of China under Grant No. 2006CB605205, the National High-Tech Research Program under Grant No. 2006AA03Z111, the National Outstanding Young Scientist Foundation under Grant No. 50525103, and the Hundred Talents Program of the Chinese Academy of Sciences.

References

[1] Mishra RS, Mahoney MW, McFadden SX, Mara NA, Mukherjee AK. Scripta Mater 1999;42:163.
[2] Benavides S, Li Y, Murr LE, Brown D, McClure JC. Scripta Mater 1999;41:809.
[3] Su JQ, Nelson TW, Sterling CJ. Philos Mag 2006;86:1.
[4] Ma ZY, Sharma SR, Mishra RS. Scripta Mater 2006;54:1623.
[5] Mishra RS, Ma ZY. Mater Sci Eng R 2005;50:III.
[6] Hirata T, Oguri T, Hagino H, Tanaka T, Chung SW, Takigawa Y, et al. Mater Sci Eng A 2007;456:344.
[7] Sutton MA, Yang B, Reynolds AP, Taylor R. Mater Sci Eng A 2002;323:160.
[8] Mahoney MW, Rhodes CG, Flintoff JG, Spurling RA, Bingel WH. Metall Mater Trans 1998;29:1955.
[9] Krishnan KN. Mater Sci Eng A 2002;327:246.
[10] Prangnell PB, Heason CP. Acta Mater 2005;53:3179.
[11] Cui GR, Ma ZY, Li SX. Scripta Mater 2008;58:1082.
[12] Field D, Nelson T, Hovanski Y, Jata K. Metall Mater Trans A 2001;32:2869.
[13] Hu H. Metall Mater Trans A 1983;14:85.
[14] Lloyd DJ, Morris LR. Acta Metall 1977;25:857.
[15] Johnston WG, Gilman JJ. J Appl Phys 1959;30:129.
[16] Lloyd DJ. Metall Trans A 1980;11:1287.
[17] Zhu H, Ghosh AK, Maruyama K. Mater Sci Eng A 2006;419:115.
[18] Robinson JM, Shaw MP. Int Mater Rev 1994;39:113.
[19] Mahoney MW, Mishra RS, Nelson T, Flintoff J, Islamgaliev R, Hovansky Y. In: Jata KV, Mahoney MW, Mishra RS, Semiatin SL, Filed DP, editors. Friction Stir Welding and Processing. Warrendale (PA): TMS; 2001. p. 183.
[20] Vilac P, Quintino L, dos Santos JF. J Mater Process Tech 2005;169:452.
[21] Tang W, Guo X, McClure JC, Murr LE. J Mater Process Manufact Sci 1999;7:163.
[22] Sakai T, Yang X, Miura H. Mater Sci Eng A 1997;234–236:857.
[23] Etter AL, Baudin T, Fredj N, Penelle R. Mater Sci Eng A 2007;445–446:94.
[24] Jata KV, Semiatin SL. Scripta Mater 2000;43:743.
[25] Ito Y, Tsuji N, Saito Y, Utsunomiya H, Sakai T. J Jpn Inst Met 2000;64:429.
[26] Sato YS, Urata M, Kokawa H, Ikeda K. Mater Sci Eng A 2003;354:298.
[27] Jin H, Lloyd DJ. Scripta Mater 2004;50:1319.
[28] Fujita H, Miyazaki S. Acta Metall 1978;26:1273.
[29] Yoshida F. Int J Plast 2000;16:359.
[30] Sun HB, Yoshida F, Ohmori M, Ma X. Mater Lett 2003;57:4535.
[31] Wen W, Morris JG. Mater Sci Eng A 2004;373:204.
[32] Li SX, Cui GR. J Appl Phys 2007;101:083525.
[33] Hayes JS, Keyte R, Prangnell PB. Mater Sci Tech 2000;16:1259.